ChemEngineering

MDPI

Article

Advanced Oxidation of PET-Derived Monomers Using Excimer Radiation and Hydrogen Peroxide: Kinetic and Operational Insights

María Gómez, María Claudia Montiel, Elisa Gómez, Asunción María Hidalgo, Fuensanta Máximo and María Dolores Murcia *

Department of Chemical Engineering, Faculty of Chemistry, Campus de Espinardo, University of Murcia, 30100 Murcia, Spain; maria.gomez@um.es (M.G.); cmontiel@um.es (M.C.M.); egomez@um.es (E.G.); ahidalgo@um.es (A.M.H.); fmaximo@um.es (F.M.)

* Correspondence: md.murcia@um.es

Abstract

Growing environmental concern over plastic pollution has increased the need to address the persistence of PET-derived monomers, such as bis(2-hydroxyethyl) terephthalate (BHET) and terephthalic acid (TPA). This work examines the use of excimer radiation lamps combined with hydrogen peroxide (H_2O_2) to enhance advanced oxidation processes (AOPs) for their degradation. This approach stands out for its high selectivity, absence of mercury, and lower production of toxic byproducts. Experimental tests assessed how different operational factors affect pollutant degradation, such as the initial pollutant concentration (50–200 mg/L), the reaction volume (125–500 mL), and the H_2O_2:monomer mass ratio (0:1–6:1 for BHET and 0:1–4:1 for TPA). For BHET, the best results occurred with a 5:1 mass ratio, while TPA degraded optimally with a 3:1 ratio, with a 250 mL reaction volume and a 100 mg/L initial concentration for both compounds. Under these conditions, total degradation of the initial monomers was achieved in around 30 and 80 min for BHET and TPA, respectively, and at the end of the reaction, COD decreased by 46% and 32% relative to their initial values. In both cases, hydrogen peroxide was crucial since UV radiation alone led to much lower degradation efficiency. These results emphasize the need to optimize operational conditions for greater efficiency and establish a starting point for future use of excimer technology in the treatment of wastewater contaminated with PET and its derivatives. Additionally, the degradation data closely matched a pseudo-first-order kinetic model ($R^2 \approx 1$), confirming its reliability for predictive analysis, which is of high importance for the simulation and optimization of the process.

Keywords: bis(2-hydroxyethyl) terephthalate; terephthalic acid; excilamps; flow-through photoreactor; kinetic model

Academic Editor: George Z. Papageorgiou

Received: 14 November 2025
Revised: 19 January 2026
Accepted: 27 January 2026
Published: 29 January 2026

1. Introduction

The widespread use of plastic products has greatly intensified pollution, leading to serious environmental concerns. Polyethylene terephthalate (PET), widely used in packaging and textiles, contributes over 70 million tons per year, representing nearly 9% of global plastic consumption and 12% of solid waste [1–3]. Polyethylene terephthalate (PET) degrades in marine environments through abiotic and biotic processes, breaking into

chemical components via hydrolysis and UV-induced photodegradation. This leads to the formation of low-molecular-weight compounds like hydroxyterephthalates and aldehydes [4,5]. While research has mainly focused on volatile, non-polar degradation products [6,7], polar water-soluble byproducts remain poorly understood despite their higher mobility, bioavailability, and potential environmental impact—revealing a critical gap in current knowledge. In particular, bis(2-hydroxyethyl) terephthalate (BHET) and terephthalic acid (TPA) have emerged as critical pollutants given that they are polar water-soluble compounds, and have been classified as emerging pollutants due to their chemical stability and persistence in the environment [8].

Pyrolysis is a promising method for converting plastic waste into valuable fuels with high energy content and lower greenhouse gas emissions. However, challenges like mixed plastic contamination and poor oil quality from PET waste hinder its efficiency. Further research is needed to improve purification, reactor design, and catalyst optimization [9]. Plastic biodegradation is an eco-friendly method that uses enzymes from microorganisms to break down plastics like PET. Organisms such as *Ideonella sakaiensis* [10], mealworms [11], and waxworms [12] show promising degradation abilities, but face challenges like slow degradation rates and limited efficiency across different plastic types. Other studies have examined the enzymatic degradation of BHET into TPA with IsPETase^{PA} and MHETase enzymes [13,14]. The main enzymes involved are PETase and MHETase, which act sequentially: PETase breaks PET into MHET, and MHETase further decomposes MHET into terephthalic acid and ethylene glycol. These can be assimilated by microorganisms or reused as recyclable monomers. Other enzymes, such as lipases, cutinases, and esterases [15–18], show similar mechanisms. Although well studied, enzymatic degradation still faces challenges of efficiency and cost to be competitive in wastewater treatment plants.

Catalytic transformation of plastic waste is a sustainable and eco-friendly alternative to traditional disposal methods. It enables the conversion of plastic trash into valuable industrial products, creating new economic opportunities. Emerging strategies include photochemistry, electrochemistry, and thermochemistry [19].

Advanced Oxidation Processes (AOPs) are widely used in wastewater treatment and other industries due to their high efficiency and low equipment costs. While single AOPs are effective, combining them often yields better results, especially for antibiotic-contaminated water [20,21]. Various AOPs, including Fenton's reaction [22], ozonation [23], and photocatalysis [24], have been studied for their efficacy in degrading persistent organic pollutants such as microplastics [25,26]. Combining excimer UV lamps with hydrogen peroxide enhances Advanced Oxidation Processes (AOPs) by generating hydroxyl radicals that enable efficient degradation of compounds such as BHET and TPA [27]. This method offers high selectivity, avoids the use of toxic mercury, and minimizes harmful byproducts compared to conventional UV treatments. Excimer lamps also present important advantages, including narrow-band UV emissions that are nearly monochromatic and closely match the dissociation energies of key organic compound bonds. Their mercury-free operation and long service life further reinforce their suitability for sustainable and effective photochemical applications [28].

Excimer radiation lamps from different sources (KrCl, XeBr, and Cl_2) have been used both in static setups [29,30] and photoreactors [31,32] to study the removal of phenolic compounds [29], dyes [30,31], and other types of emerging contaminants [32], achieving total degradation in the optimal conditions in all cases. In a previous study [27] investigating the photodegradation of BHET and TPA using static KrCl and XeBr excimer lamps, the KrCl lamp (222 nm) exhibited superior efficiency and effectiveness, attributed to its optimal spectral overlap with H_2O_2 and enhanced hydroxyl radical generation, totally degrading both PET-derived monomers, while XeBr only attained complete removal of

BHET at longer times. Building upon these findings, a KrCl exciplex flow-through photoreactor was employed to further examine the removal of these microplastics. To the best of our knowledge, no kinetic studies have been published on the oxidation of BHET and PET using this type of excimer lamp. In this context, the present work aims to test the new excilamp configuration that would allow for continuous scale-up of the process, as well as to validate a previously developed kinetic model for the system under study. The calculation of the involved kinetic parameters will facilitate the simulation of the photodegradation reaction in many different conditions and its subsequent optimization.

2. Materials and Methods

2.1. Materials

Terephthalic acid (TPA, 98% purity) and bis(2-hydroxyethyl) terephthalate (BHET, 85% purity) were supplied by Sigma-Aldrich (St. Louis, MO, USA) and served as the model PET-derived pollutants. The oxidizing agent, H_2O_2 (33% *w*/*v*), was obtained from PanReac AppliChem (Barcelona, Spain). To improve the solubility of the monomers, a 0.1 M phosphate buffer solution (pH 7.0) was selected as the solvent. This buffer was formulated by combining specific volumes of 0.1 M Na_2HPO_4 (Sigma-Aldrich) and 0.1 M NaH_2PO_4 (PROBUS, S.A., Badalona, Spain). Periodic checks of the H_2O_2 stock concentration were performed using titration with $KMnO_4$ PanReac AppliChem (Barcelona, Spain). For the HPLC mobile phase preparation, HPLC-grade acetonitrile, ultrapure water, and 98% H_2SO_4 were required.

2.2. Experimental Setup

A flow-through KrCl photoreactor (222 nm) supplied by the High Current Electronics Institute (Tomsk, Russia) was the primary piece of equipment for these experiments. Its irradiation zone, measuring 30 cm in length and 2 cm in internal diameter, provided an irradiation area of 188.5 cm^2. The average radiation intensity, as specified by the manufacturer, was 2.38 $mWcm^{-2}$. The experimental procedure involved pumping a solution of the microplastic compound and reagents (e.g., hydrogen peroxide) from a stirred tank into the photoreactor. The reactor's effluent was continuously recirculated to the tank, thereby operating the system as a pseudo-batch reactor. The operational parameters for all experiments were a room temperature of 23–25 °C and a total duration of 120 min. The pump flow rate was kept constant at 20 rpm.

Figure 1 depicts the experimental equipment, including all its main components. Samples were collected at specific reaction times: 0, 1, 2, 3, 5, 10, 15, 20, 30, 40, 60, 90, and 120 min. Experiments were performed in triplicate, and the average value is reported with an error of less than 5%.

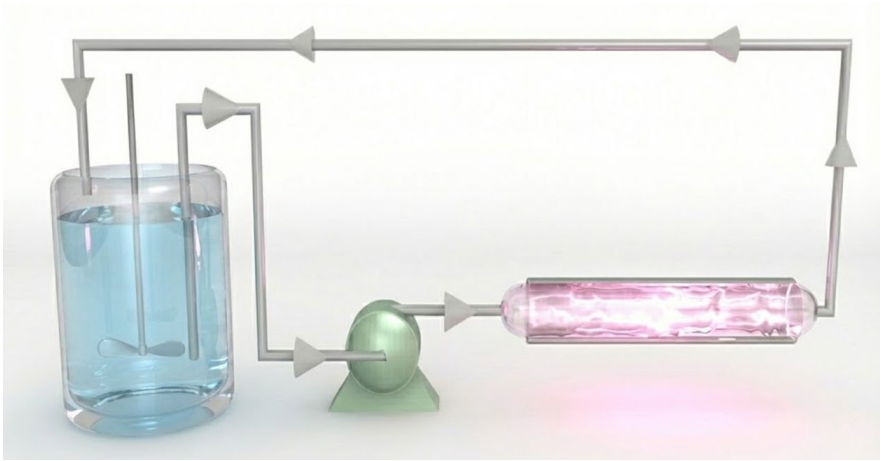

Figure 1. KrCl flow-through photoreactor experimental scheme.

https://doi.org/10.3390/chemengineering10020019

2.3. Experimental Design

To evaluate how key operational parameters influence the degradation of TPA and BHET, three series of experiments were performed, focusing on the H_2O_2–monomer mass ratio, initial monomer concentration, and reaction volume. During each run, 500 µL aliquots were withdrawn at set time intervals and promptly prepared for analysis. Table 1 summarizes all experimental conditions applied to the KrCl flow-through photoreactor system.

Table 1. Experimental conditions for all series with KrCl flow-through photoreactor.

Monomer	Experiment Number	Mass Ratio [H_2O_2]: [Monomer]	[Monomer]$_0$ (mg/L)	[H_2O_2]$_0$ (mg/L)	V (mL)
BHET	1	0:1	100	0	250
	2	1:1		100	
	3	2:1		200	
	4	3:1		300	
	5	4:1		400	
	6	5:1		500	
	7	6:1		600	
	8	5:1	50	250	250
	9		100	500	
	10		150	750	
	11		200	1000	
	12	5:1	100	500	125
	13				250
	14				375
	15				500
TPA	1	0:1	100	0	250
	2	1:1		100	
	3	2:1		200	
	4	3:1		300	
	5	4:1		400	
	6	3:1	50	150	250
	7		100	300	
	8		150	450	
	9		200	600	
	10	3:1	100	300	125
	11				250
	12				375
	13				500

2.4. Analytical Methods

2.4.1. Monomer Quantification

The analysis of TPA and BHET concentrations was performed via a Waters HPLC system (Alliance iS HPLC System Software Version 2.0, Waters Corporation, Milford, MA, USA). The system configuration included a Waters 600 controller, a 717 plus autosampler, and a 2996 PDA detector, with data acquisition and processing handled by Waters Empower 2 software (version 2.0). Isocratic chromatographic separation utilized a C18 column, and the mobile phase consisted of 60% ultrapure water, 20% acetonitrile, and 20% of a 10 mM H_2SO_4 aqueous solution. Operational parameters featured a 1.0 mL min^{-1} flow

rate and a 20 µL injection volume. For quantification, the peak area at the maximum absorbance wavelength for each compound was integrated and compared against a calibration curve developed using external standards. A chromatogram illustrating the respective retention times for each compound is presented in Figure 2.

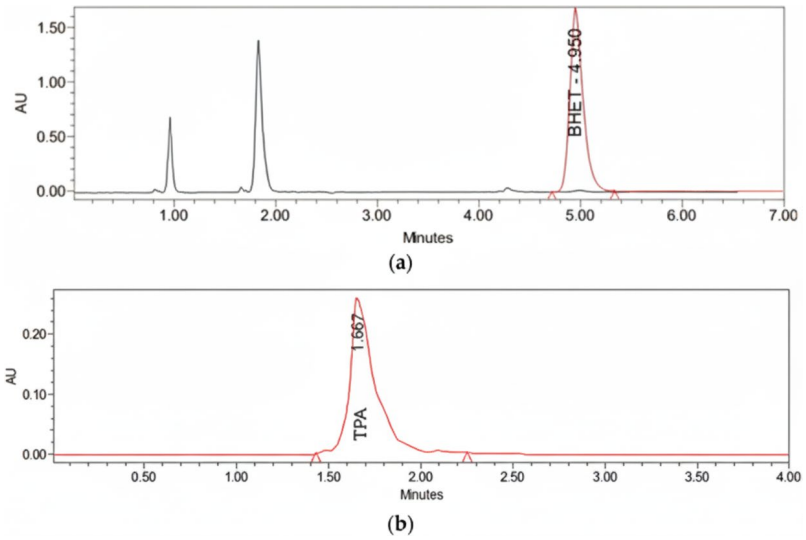

Figure 2. Examples of chromatograms: (**a**) BHET (**b**) TPA.

2.4.2. Chemical Oxygen Demand Quantification

The degree of mineralization of organic contaminants was assessed through Chemical Oxygen Demand (COD) measurements using a Hanna Instruments HI 83,099 multiparameter photometer (Woonsocket, RI, United States) together with an HI 839,800 COD reactor (Woonsocket, RI, United States). COD analyses were conducted on selected samples—most often those corresponding to the H_2O_2/Monomer Mass Ratio experiments—after 120 min of reaction time. The procedure was based on the conventional dichromate colorimetric technique, employing low-range (LR) reagent vials. To ensure that the resulting COD readings remained within the calibrated limits of the device, the samples were diluted beforehand with ultrapure water at 1:2 and 1:4 ratios. The COD tests were performed in duplicate, and the average value is reported with an error of less than 5%.

3. Results and Discussion

In all the Figures, conversion, calculated as the ratio between the monomer initial concentration minus concentration at a given time and its initial concentration, is represented versus reaction time. In Sections 3.1–3.3, the dots in the graphs represent the experimental data, and the solid line fitted to the model is explained in Section 3.4.

3.1. Effect of H_2O_2–Monomer Mass Ratio

The impact of the H_2O_2-to-monomer mass ratio on degradation efficiency underscores the pivotal role of hydrogen peroxide as a source of hydroxyl radicals (Figure 3a,b). Direct photolysis at a 0:1 ratio, in the absence of H_2O_2, severely limited the degradation of both substrates, demonstrating that direct UV photon absorption by TPA and BHET is kinetically insufficient for substantial mineralization. After a 120 min treatment period, TPA conversion remained minimal at 15.30%, whereas BHET exhibited a significantly higher lability to radical oxidation with a 69.7% removal rate. This kinetic disparity aligns with prior findings reported in [27], where similar results showed ~60% removal for BHET and only 0.14% for TPA under static lamp conditions. This divergence is chemically rooted: TPA possesses a highly resonant benzene ring system, conferring higher bond

dissociation energy and a smaller reaction cross-section towards OH· radicals compared to the more accessible aliphatic sites on BHET. Consequently, TPA exhibits greater recalcitrance to photolytically induced radical attack. In fact, TPA, due to its stability, has been used as a radical scavenger, and it is known to react with hydroxyl radicals to form a stable fluorescent product instead of mineralizing [33]. Also, some studies [34] have shown that TPA degrades better at around 240 nm.

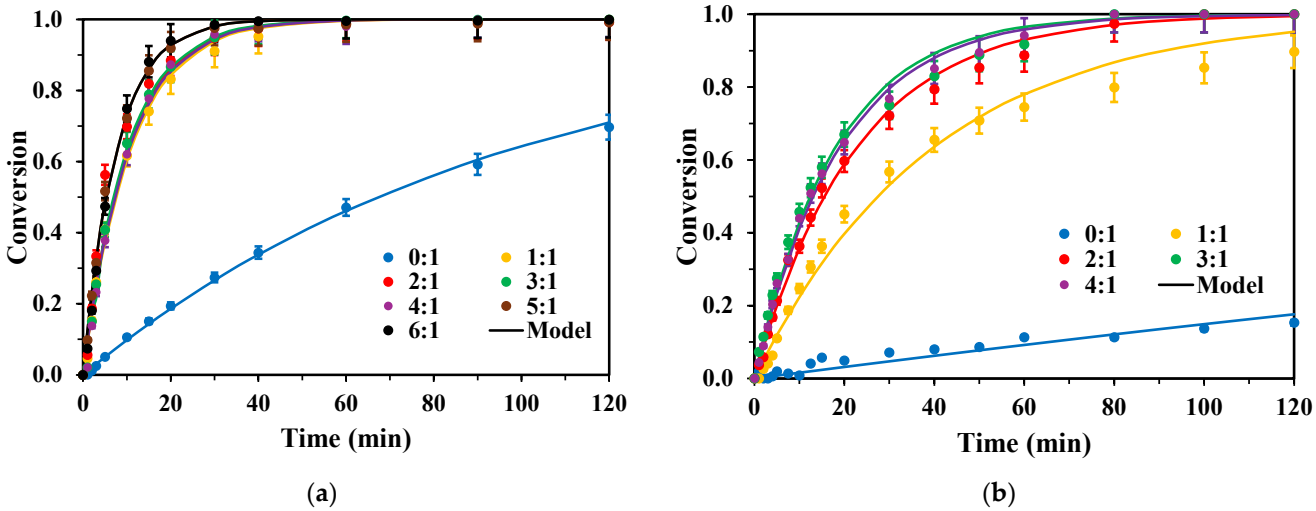

Figure 3. Experimental and calculated conversion rates versus time for the different compounds in the KrCl excilamp varying H_2O_2–monomer mass ratios, $[Monomer]_0$ = 100 mg/L, V_R = 250 mL, for (**a**) BHET and (**b**) TPA.

In the case of the BHET monomer (Figure 3a), the degradation efficiency exhibited a substantial enhancement upon the addition of hydrogen peroxide (H_2O_2) as an oxidizing agent. It was observed that as the H_2O_2–BHET mass ratio increased throughout the experiments, the degradation rate improved, leading to maximum conversion in progressively shorter times. In the experiment with a mass ratio of H_2O_2–BHET of 4:1, full conversion was reached 30 min after the reaction began. This conversion time was further reduced to 20 min in the final experiment, which employed a 6:1 mass ratio. For the TPA monomer (Figure 3b), as the mass ratio increased, the overall efficiency improved as well, with complete contaminant degradation occurring in shorter times. Experimental results show that ratios of 3:1 and 4:1 yield similar conversion behavior, with nearly overlapping conversion curves. This behavior agrees with that observed in previous studies [27] where, for the highest ratios H_2O_2–monomer tested, H_2O_2 acts as a scavenger of hydroxyl radicals, thus leading to no improvement of the process.

Taking into account the mineralization reactions,

$$C_8H_6O_4\ (TPA) + 15H_2O_2 \rightarrow 8CO_2 + 18H_2O$$

$$C_{12}H_{14}O_6\ (BHET) + 25H_2O_2 \rightarrow 12CO_2 + 32H_2O,$$

and considering the molar masses (TPA: 166 g/mol, BHET: 254 g/mol), the stoichiometric mass ratio of substrate to H_2O_2 for complete mineralization would be 3.07 and 3.35, respectively. This suggests that the optimal mass ratio should be slightly higher than the theoretical value, at approximately 3. Further increases in the mass ratio would likely result in similar conversion values and overlapping degradation curves. However, excess hydrogen peroxide would remain in the medium, thereby increasing the COD (Chemical Oxygen Demand) since it is a reagent that consumes oxygen during the reaction. To determine the optimal ratio, COD analysis was performed on the different experiments in

this series, with samples taken at the end of the reaction (after 2 h of operation). These results are presented in Figure 4. The initial COD was also determined, yielding a value of 144.5 mg/L for TPA and 157.3 mg/L BHET, both at initial concentrations of 100 mg/L.

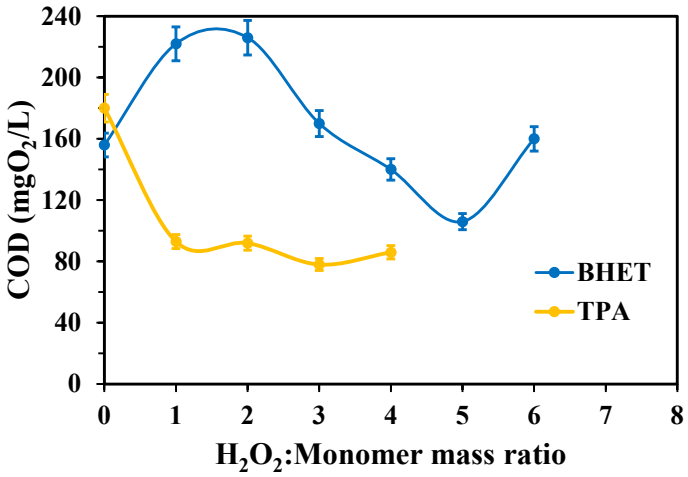

Figure 4. Chemical oxygen demand after irradiation of samples with different H_2O_2–compound mass ratios.

Attention must be given to the COD values starting from the H_2O_2–BHET mass ratio of 4:1, which corresponds to the mass ratio immediately above the stoichiometric ratio (3.35). Selecting a lower ratio would be impractical, as it would not ensure complete oxidation of the contaminant prior to reaching the stoichiometric point. Therefore, based on the data presented in Figure 4, the 5:1 ratio is selected. Although it exceeds the theoretical value, this is common practice given that additional peroxide is typically required to oxidize intermediate degradation photoproducts such as mono-(2-hydroxyethyl) terephthalate (MHET) and, eventually, TPA, which will ultimately break into short-length carboxylic acids [34]. This 5:1 ratio yields the lowest COD value (106 mgO_2/L, COD decrease of 32%), thereby confirming the complete degradation of BHET and the effective breakdown of most intermediate photoproducts, making it the optimal mass ratio. A higher mass ratio of 6:1 shows an increase in COD (160 mgO_2/L), suggesting an excess of hydrogen peroxide in the reaction. Although the contaminant is fully oxidized, the surplus peroxide contributes to a higher COD value and represents an unnecessary consumption of the oxidizing agent. In the case of TPA, the focus must be on the COD values from the 3:1 (78 mgO_2/L) and 4:1 (86 mgO_2/L) H_2O_2–TPA experiments. Since both ratios yield similar conversion rates, as shown in Figure 3b, the optimal ratio is identified by the lower COD value found in the 3:1 case, which achieves a 46% COD decrease. The higher COD observed at the 4:1 ratio indicates an unnecessary excess of oxidant in the reaction medium. It is interesting to note that the optimal mass ratio of H_2O_2–monomer, with respect to the theoretical one, is higher in the case of BHET. This finding corresponds with the fact that photodegradation for this monomer is faster and more efficient, with higher intermediate COD values obtained, suggesting that more intermediate photoproducts are formed and more hydrogen peroxide is required to oxidize them. A reduction in COD is commonly used as an indirect indicator of decreased toxicity since many toxic organic pollutants contribute strongly to the oxygen demand of wastewater. Thus, the marked decrease in COD after treatment reflects a substantial removal of oxidizable and potentially toxic compounds, so it can be assumed that the remaining products are less harmful than the initial mixture.

Therefore, an optimum mass ratio for H_2O_2–monomer of 5:1 and 3:1 for BHET and TPA, respectively, is chosen for the rest of the experiments. This is in concordance with

the previous results found for the static experimentation [27]. Moreover, the apparent quantum yields (AQYs) of both BHET and TPA rise sharply when hydrogen peroxide is added due to the formation of hydroxyl radicals. BHET increases from 1.2% under direct photolysis to 4.6% with the optimal mass ratio of H_2O_2–BHET, while TPA rises from 0.39% to 4.6% also for its optimal mass ratio for H_2O_2–TPA under similar conditions. These enhancements show that H_2O_2 introduces an additional oxidative pathway that accelerates degradation beyond direct photolysis.

3.2. Effect of Initial Monomer Concentration

The effect of the initial BHET concentration (Figure 5a) and initial TPA concentration (Figure 5b) was investigated at the corresponding optimal H_2O_2–monomer ratios of 5:1 for BHET and 3:1 for TPA.

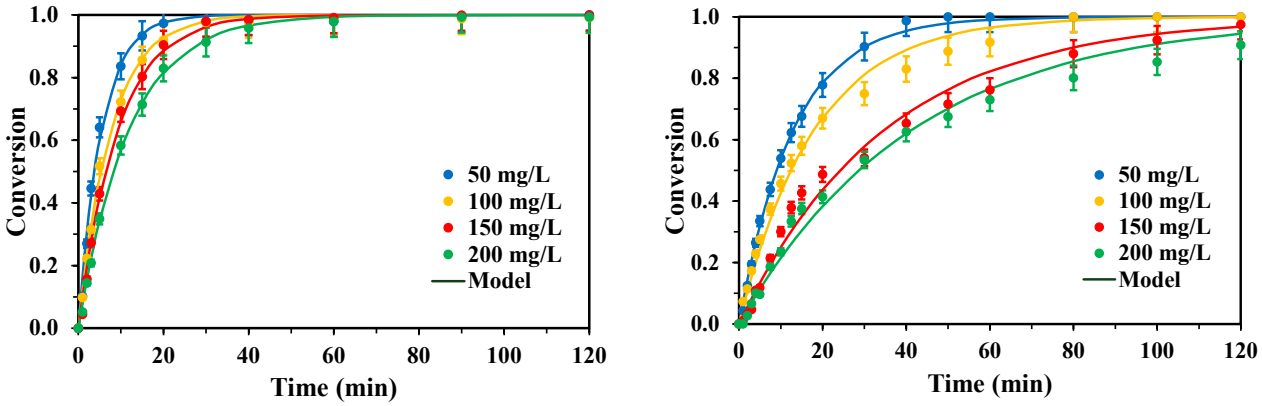

Figure 5. Experimental and calculated conversion rates versus time for the different compounds in the KrCl excilamp with varying initial compound concentrations, V_R = 250 mL: (**a**) H_2O_2–BHET mass ratio of 5:1; (**b**) H_2O_2–TPA mass ratio of 3:1.

A distinct inverse relationship was observed between the initial monomer concentration and the degradation rate for both compounds, as expected, since the same UV radiation intensity is available, so higher initial concentrations lead to lower availability of hydroxyl radicals and lower conversion values. The inner filter effect must also be considered at higher compound concentrations, leading the monomers to shield hydrogen peroxide so that fewer hydroxyl radicals are formed [35]. For both compounds (Figure 5a,b), degradation was fastest at the lowest initial concentration. The BHET monomer (Figure 5a) achieved almost complete conversion (>97%) at 50 mg L^{-1} in under 20 min. As the initial concentration increased to 150 and 200 mg L^{-1}, the degradation slowed, reaching the same final concentration within 30 and 60 min. For the TPA monomer (Figure 5b), for the lowest concentration of 50 mg L^{-1}, 40 min is needed to reach 98% conversion, and this time increases to 120 min with an initial TPA concentration of 150 mg L^{-1}. The highest TPA initial concentration does not totally degrade the compound after two hours of treatment.

3.3. Effect of Reaction Volume

Variation in the reaction volume between 125 and 500 mL is depicted in Figure 6a,b for both BHET and TPA monomers.

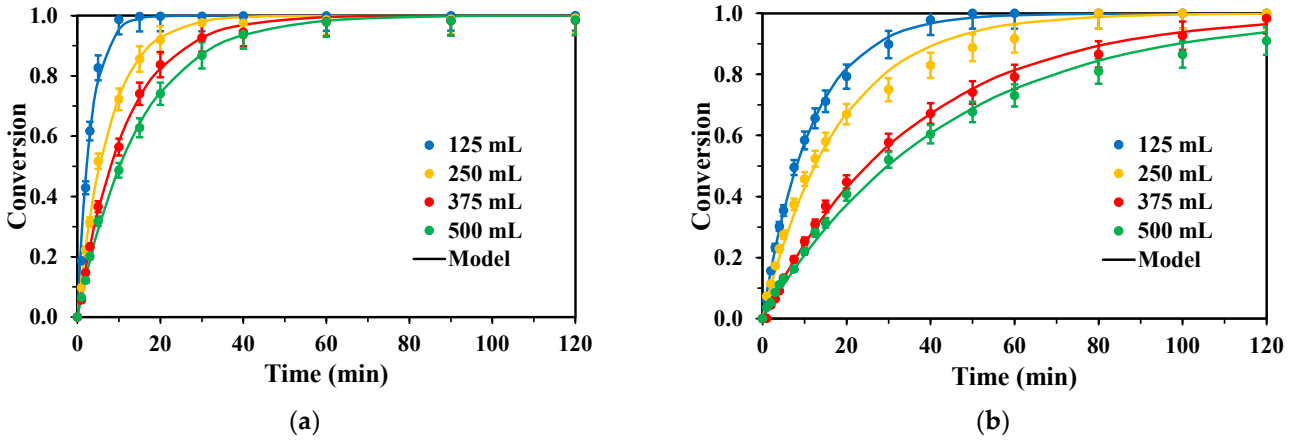

Figure 6. Experimental and calculated conversion rates versus time for the different compounds in the KrCl excilamp with varying reaction volumes, $[Monomer]_0$ = 100 mg/L: (**a**) H_2O_2–BHET mass ratio of 5:1; (**b**) H_2O_2–TPA mass ratio of 3:1.

As can be observed in Figure 6, the degradation rate increases as the reaction volume decreases, as expected. Given that the initial contaminant concentration remains constant across all experiments, larger reaction volumes result in fewer recirculation cycles of the solution. Consequently, the exposure time of each molecule to the lamp's emitted light is reduced, leading to lower degradation efficiency. This phenomenon is attributed to the higher UV energy density per unit volume in smaller reaction systems, which accelerates the degradation process.

In the experiment with the smallest reaction volume (125 mL), maximum conversion was achieved within just 20 min of operation for the BHET monomer and 40 min for the TPA monomer. In contrast, the remaining experiments for BHET required approximately one hour to reach the same level of conversion and two hours in the case of TPA. Therefore, larger reaction volumes are associated with slower conversion rates, indicating reduced irradiation efficiency and significantly lower contaminant degradation. These results agree with previous studies carried out with excilamps with different types of organic pollutants [29–32].

3.4. Model Fitting of the KrCl Flow-Through Photoreactor Results

The kinetic description adopted in this work stems from an earlier model [30], later reshaped for operation in a photoreactor treating dyes such as amaranth [31] and other organic molecules. In this reinterpretation, the liquid medium is divided into two conceptual zones that differ in the concentration of the target species. The first is a very thin irradiated layer, where the photochemical transformation occurs, and only minimal amounts of the unreacted compound remain. The second corresponds to the well-mixed bulk region, which maintains a uniform concentration that progressively declines during the reaction and represents the value obtained experimentally.

Within this scheme, the rate constant behaves as a function of several operational factors. Consequently, the system does not follow a strict first-order kinetic law; instead, it displays a pseudo-first-order response.

The mentioned pseudo-first-order kinetic fit was applied to the data for each experimental series performed, using the following model equation:

$$X = 1 - e^{-k_r t} \quad (1)$$

The fitting procedure was conducted using the "Curve Expert" 14.0 program. Experimental time (in minutes) and conversion data were input, the model equation was

selected, and the program executed the fitting algorithm. The software calculates the apparent kinetic constant (k_r) from the experimental conversion data. This constant is then used in the model equation to generate the theoretical conversion values. The program further provides the correlation coefficient for every fit performed.

The experimental conversion data are represented by the points in Figures 3, 5, and 6, while the solid curves depict the model predictions generated from Equation (1).

Table 2 compiles the pseudo-first-order kinetic constants, k_r, derived from fitting each experimental series to the model, along with the corresponding correlation coefficients. Both the graphical results and the numerical values in Table 2 clearly indicate that the proposed model reproduces the experimental behavior with excellent accuracy.

Table 2. Pseudo-first-order kinetic constant, k_r, for the two monomers.

BHET			TPA		
Experiment Number	**k_r (min^{-1})**	**r**	**Experiment Number**	**k_r (min^{-1})**	**r**
1	0.0103	0.9994	1	0.0016	0.9427
2	0.0926	0.9984	2	0.0253	0.9927
3	0.0979	0.9946	3	0.0444	0.9978
4	0.1010	0.9981	4	0.0556	0.9956
5	0.1123	0.9981	5	0.0530	0.9985
6	0.1310	0.9977	6	0.0771	0.9993
7	0.1280	0.9982	7	0.0566	0.9956
8	0.0184	0.9972	8	0.0287	0.9926
9	0.1310	0.9977	9	0.0242	0.9923
10	0.1080	0.9988	10	0.0855	0.9993
11	0.0843	0.9994	11	0.0556	0.9956
12	0.3050	0.9966	12	0.0280	0.9987
13	0.1310	0.9977	13	0.0233	0.9975
14	0.0869	0.9992			
15	0.0682	0.9994			

The general theoretical expression of the apparent kinetic constant, k_r, obtained through the material balance as detailed in previous studies [30,31], can be rewritten as:

$$k_r = \frac{V_r k_{c1} \varepsilon k_E k_L a I + V_r k_{c2} \varepsilon k_E k_L a I k_{lim} C_{(H_2O_2)_0}}{V \varepsilon k_E k_L a I + V k_{c1} C_0 + V k_{c2} k_{Lim} C_{(H_2O_2)_0} C_0} \quad (2)$$

For the model fitting of experimental series 1, by putting all constants together, the following dependence with $[H_2O_2]_0$ is obtained:

$$k_r = \frac{a + b\,[H_2O_2]_0}{c + d\,[H_2O_2]_0} \quad (3)$$

Figure 7 shows the fitting to this previous equation for series 1 using the different values of mass ratio $[H_2O_2]_0$–[monomer] and the calculated values of k_r. The values of the different parameters of Equation (3) are presented in Table 3. In Figure 7, it is also important to point out the much higher values of k_r obtained for the BHET compound than for TPA, which agrees with the experimental results, whereby more efficient and faster degradation was attained for this monomer.

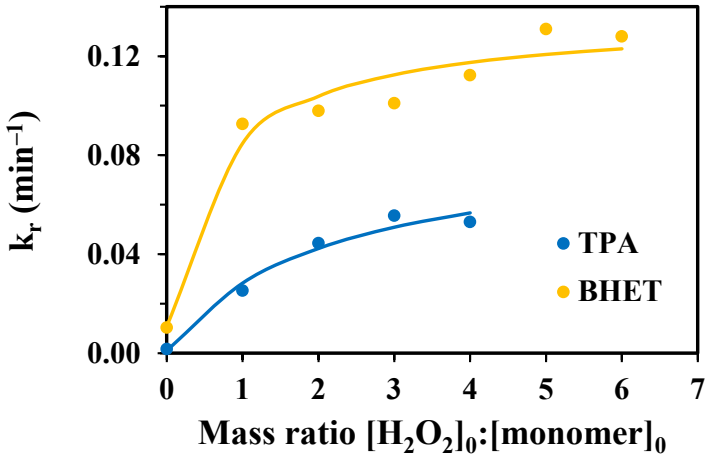

Figure 7. Influence of H_2O_2–monomer mass ratio on the apparent kinetic constant for the KrCl flow-through photoreactor.

Table 3. Fitting of k_r to Equation (3). Calculated parameters for KrCl flow-through photoreactor.

Parameter	TPA	BHET
a	0.0054	0.0211
b	0.0227	0.3880
c	5.5517	1.9400
d	2.6257	2.8500
r	0.9880	0.9800

For the analysis of experimental series 2—focused on examining how variations in the initial concentration of the compound influence the system—a reformulated expression can be derived from Equation (2) to enable its incorporation into the kinetic model.

$$\frac{1}{K_r} = \frac{V}{V_r k_{c1}} + \frac{V}{V_r k_{c1} \varepsilon k_E k_L a I} C_0 \quad (4)$$

Figure 8 illustrates the strong agreement between experimental data and Equation (4). The plot also reveals the expected trend: the pseudo-first-order constant k_r decreases as the initial monomer concentration increases. In addition, the k_r values obtained for the BHET experiments are consistently higher than those corresponding to TPA, which is fully consistent with the observed experimental behavior.

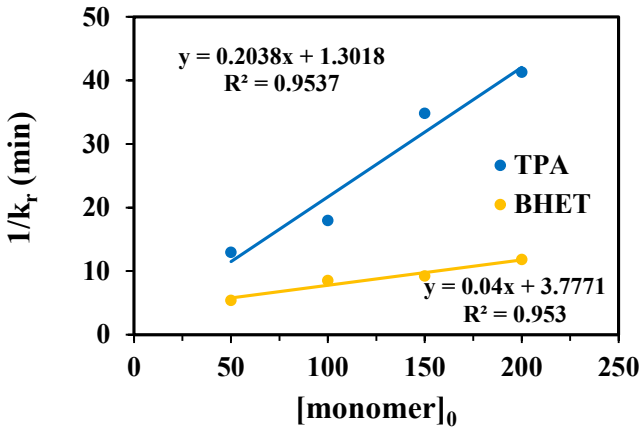

Figure 8. Influence of $[compound]_0$ on the apparent kinetic constant for the KrCl flow-through photoreactor.

In the third series, a linear variation of k_r with an inverse volume is initially expected according to the following expression derived, again, from Equation (2):

$$k_r = \frac{V_r k_{c1} \varepsilon k_E k_L a I + V_r k_{c2} \varepsilon k_E k_L a I k_{lim} C_{(H_2O_2)lim}}{\varepsilon k_E k_L a I + k_{c1} C_0 + k_{c2} C_0 k_{lim} C_{(H_2O_2)lim}} \times \frac{1}{V} \quad (5)$$

Figure 9 depicts the fitting of the apparent kinetic constant to the inverse volume for the BHET and TPA compounds according to the previous equation. As in the previous series, the results obtained from the model agree with the experimental ones, and the values of k_r are higher for the BHET assays.

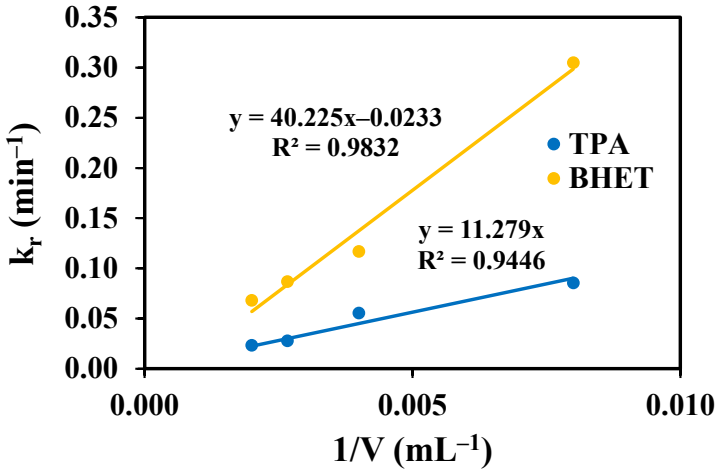

Figure 9. Influence of reaction volume on the apparent kinetic constant for the KrCl flow-through photoreactor.

4. Conclusions

The findings of this study demonstrate the efficient degradation of BHET and TPA achieved through the use of a KrCl photoreactor. The results indicate that the optimal H_2O_2–monomer mass ratio for the total degradation of BHET is 5:1 and for TPA is 3:1. At a reaction volume of 250 mL and initial monomer concentrations of 100 mg/L, these conditions yielded the lowest COD values (reductions of 46 and 32%, respectively), with no presence of intermediate compounds at the end of the reaction and minimal excess oxidant.

Additionally, a kinetic model, previously developed by the authors, has been tested and validated with excellent fitting of all experimental data. This model agrees with the observed dependence of the pseudo-first-order kinetic constant on different experimental variables. In this manner, the apparent kinetic constant of the reaction is affected by both the initial concentration of the compound and the reaction volume. Overall, the findings emphasize the importance of optimizing the H_2O_2–monomer mass ratio and understanding the kinetics of the reaction in enhancing the efficiency of organic pollutant mineralization in the photoreactor system.

Owing to its demonstrated efficiency and reliability, further investigation is recommended to assess its scalability, long-term operational stability, and potential for implementation in real-world wastewater treatment applications. Additionally, more research is needed to determine the nature of the intermediate products and test more conditions, assessing their economic viability and environmental impact. Research into the combination of Advanced Oxidation Processes (AOPs) with other treatment methods could provide insights into achieving higher efficiencies in pollutants and their intermediates removal.

https://doi.org/10.3390/chemengineering10020019

Author Contributions: conceptualization, E.G., F.M. and M.G.; methodology, A.M.H., M.C.M. and M.D.M.; formal analysis, E.G., A.M.H. and M.C.M.; investigation, F.M., M.G. and M.D.M.; resources, M.G. and M.D.M.; data curation, F.M.; A.M.H. and M.C.M.; writing—original draft preparation, M.G. and M.D.M.; writing—review and editing, A.M.H. and M.C.M.; visualization, F.M.; supervision, E.G.; project administration, M.G.; funding acquisition, M.G., M.C.M. and M.D.M. All authors have read and agreed to the published version of the manuscript.

Funding: This study forms part of the ThinkInAzul programme and was supported by MCIU with funding from European Union NextGenerationEU (PRTR-C17.I1) and by Comunidad Autónoma de la Región de Murcia—Fundación Séneca.

Data Availability Statement: The data presented in this study are available upon request to the corresponding author.

Conflicts of Interest: The authors declare no conflicts of interest. The funders had no role in the design of the study; in the collection, analyses, or interpretation of data; in the writing of the manuscript; or in the decision to publish the results.

Abbreviations

The following abbreviations are used in this manuscript:

a	Parameter of Equation (3), (mg L^{-1} min^{-2})
b	Parameter of Equation (3), (mg L^{-1} min^{-2})
c	Parameter of Equation (3), (mg L^{-1} min^{-1})
d	Parameter of Equation (3), (mg L^{-1} min^{-1})
ε	Quantum yield, (mg L^{-1} W^{-1})
I	Intensity of radiation, (w)
k_{c1}	Kinetic constant of direct photolysis in the film, (min^{-1})
k_{c2}	Kinetic constant with hydrogen peroxide in the film, ($mg^{-1}L^{-1}min^{-1}$)
k_E	Proportionality constant, (dimensionless)
k_La	Volumetric mass transfer coefficient, (min^{-1})
k_{lim}	Proportionality constant between initial H_2O_2 concentration and H_2O_2 concentration in the film
k_r	Pseudo first order kinetic constant, (min^{-1})
t	Reaction time, (min)
V	Volume of bulk solution, (mL)
V_r	Volume of photoreaction zone in the film, (mL)
X	Conversion of monomer, (dimensionless)
C_0	Initial concentration of monomer, (mgL^{-1})
$C_{(H_2O_2)_0}$	Initial concentration of hydrogen peroxide, (mgL^{-1})
$C_{(H_2O_2)_{lim}}$	Concentration of hydrogen peroxide in the film, (mgL^{-1})

References

1. Tournier, V.; Topham, C.M.; Gilles, A.; David, B.; Folgoas, C.; Moya-Leclair, E.; Kamionka, E.; Desrousseaux, M.L.; Texier, H.; Gavalda, S.; et al. An engineered PET depolymerase to break down and recycle plastic bottles. *Nature* **2020**, *580*, 216–219. https://doi.org/10.1038/s41586-020-2149-4.
2. Volpe, V.; Lanzillo, M.S.; Molaro, A.; Affinita, G.; Pantani, R. Characterization of recycled/virgin polyethylene terephthalate composite reinforced with glass fiber for automotive applications. *J. Compos. Sci.* **2022**, *6*, 59. https://doi.org/10.3390/jcs6020059.
3. Koshti, R.; Mehta, L.; Samarth, N. Biological recycling of polyethylene terephthalate: A mini-review. *J. Polym. Environ.* **2018**, *26*, 3520–3529. https://doi.org/10.1007/s10924-018-1214-7.
4. Gewert, B.; Plassmann, M.M.; MacLeod, M. Pathways for degradation of plastic polymers floating in the marine environment. *Environ. Sci. Process. Impacts* **2015**, *17*, 1513–1521. https://doi.org/10.1039/C5EM00207A.
5. Sharma, S.; Bhardwaj, A.; Thakur, M.; Saini, A. Understanding microplastic pollution of marine ecosystem: A Review. *Environ. Sci. Pollut. Res.* **2024**, *31*, 41402–41445. https://doi.org/10.1007/s11356-023-28314-1.

6. Li, B.; Wang, Z.W.; Lin, Q.B.; Hu, C.Y. Study of the migration of stabilizer and plasticizer from polyethylene terephthalate into food simulants. *J. Chromatogr. Sci.* **2016**, *54*, 939–951. https://doi.org/10.1093/chromsci/bmw025.
7. Thoden van Velzen, E.U.; Brouwer, M.T.; Stärker, C.; Welle, F. Effect of recycled content and rPET quality on the properties of PET bottles, Part II: Migration. *Packag. Technol. Sci.* **2020**, *33*, 359–371. https://doi.org/10.1002/pts.2528.
8. Petrović, M.; Barceló, D. Introduction—Emerging pollutants in water: Threats, challenges, and research needs. In *Emerging Pollutants*; Barceló, D., Ed.; Springer: Cham, Switzerland, 2025; pp. 1–34. https://doi.org/10.1007/978-3-031-71758-1_1
9. Abbas-Abadi, M.S.; Ureel, Y.; Eschenbacher, A.; Vermeire, F.H.; Varghese, R.J.; Oenema, J.; Stefanidis, G.D.; Van Geem, K.M. Challenges and opportunities of light olefin production via thermal and catalytic pyrolysis of end-of-life polyolefins: Towards full recyclability. *Prog. Energy Combust. Sci.* **2023**, *96*, 101046. https://doi.org/10.1016/j.pecs.2022.101046.
10. Mudondo, J.; Lee, H.S.; Jeong, Y.; Kim, T.H.; Kim, S.; Sung, B.H.; Park, S.H.; Park, K.; Cha, H.G.; Yeon, Y.J.; Kim, H.T. Recent advances in the chemobiological upcycling of polyethylene terephthalate (PET) into value-added chemicals. *J. Microbiol. Biotechnol.* **2022**, *33*, 1–14. https://doi.org/10.4014/jmb.2208.08048.
11. He, L.; Yang, S.S.; Ding, J.; He, Z.L.; Pang, J.W.; Xing, D.F.; Zhao, L.; Zheng, H.S.; Ren, N.Q.; Wu, W.M. Responses of gut microbiomes to commercial polyester polymer biodegradation in *Tenebrio molitor* Larvae. *J. Hazard. Mater.* **2023**, *457*, 131759. https://doi.org/10.1016/j.jhazmat.2023.131759.
12. Ali, S.S.; Elsamahy, T.; Zhu, D.; Sun, J. Biodegradability of polyethylene by efficient bacteria from the guts of plastic-eating waxworms and investigation of its degradation mechanism. *J. Hazard. Mater.* **2023**, *443*, 130287. https://doi.org/10.1016/j.jhazmat.2022.130287.
13. Gao, Y.; Zheng, Y.; Qi, Z.; Pan, Y.; Zhou, Y.; You, S.; Su, R.; Qi, W.; Wang, M. Enhancing the biodegradation of bis(2-hydroxyethyl) terephthalate by an IsPETasePA and MHETase dual-enzyme system. *J. Chem. Technol. Biotechnol*. **2024**, *99*, 1860–1870. https://doi.org/10.1002/jctb.7688.
14. Ermis, H. A mini-review on the role of PETase in polyethylene terephthalate degradation. *Rev. Environ. Sci. Biotechnol*. **2025**, *24*, 545–555. https://doi.org/10.1007/s11157-025-09737-3.
15. Świderek, K.; Velasco-Lozano, S.; Galmés, M.A.; Olazabal, I.; Sardon, H.; López-Gallego, F.; Moliner, V. Mechanistic studies of a lipase unveil effect of pH on hydrolysis products of small PET modules. *Nat. Commun*. **2023**, *14*, 3556. https://doi.org/10.1038/s41467-023-39201-1.
16. Aristizábal-Lanza, L.; Mankar, S.V.; Tullberg, C.; Zhang, B.; Linares-Pastén, J.A. Comparison of the enzymatic depolymerization of polyethylene terephthalate and AkestraTM using *Humicola insolens* cutinase. *Front. Chem. Eng*. **2022**, *4*, 1048744. https://doi.org/10.3389/fceng.2022.1048744.
17. Veeramalli, N.S.; Aravind Kumar, J.; Vasamsetti, S.S.; Sathish, S.; Venkatesan, D.; Prabu, D.; Samrot, A.V. Microbial and enzymatic biodegradation of microplastics and nanoplastics: Advances, challenges, and sustainable solutions for environmental remediation. *Desalination Water Treat.* **2025**, *324*, 101450. https://doi.org/10.1016/j.dwt.2025.101450.
18. Raoufi, H.; Taqwa, S.; Fagiryaar, F. Enzymatic degradation of polyethylene and polyethylene terephthalate: A mini review. *Am. J. Environ. Clim.* **2023**, *2*, 41–50. https://doi.org/10.54536/ajec.v2i3.1937.
19. Li, X.; Wang, J.; Zhang, T.; Yang, S.; Sun, M.; Qian, X.; Wang, T.; Zhao, Y. Sustainable catalytic strategies for the transformation of plastic wastes into valued products. *Chem. Eng. Sci.* **2023**, *276*, 118729. https://doi.org/10.1016/j.ces.2023.118729.
20. Pandis, P.K.; Kalogirou, C.; Kanellou, E.; Vaitsis, C.; Savvidou, M.G.; Sourkouni, G.; Zorpas, A.A.; Argirusis, C. Key points of advanced oxidation processes (AOPs) for Wastewater, organic pollutants and pharmaceutical waste treatment: A mini review. *ChemEngineering* **2022**, *6*, 8. https://doi.org/10.3390/chemengineering6010008.
21. Kim, S.; Sin, A.; Nam, H.; Park, Y.; Lee, H.; Han, C. Advanced oxidation processes for microplastics degradation: A recent trend. *Chem. Eng. J. Adv.* **2022**, *9*, 100213. https://doi.org/10.1016/j.ceja.2021.100213.
22. Bule Možar, K.; Miloloža, M.; Martinjak, V.; Radovanović-Perić, F.; Bafti, A.; Ujević Bošnjak, M.; Markić, M.; Bolanča, T.; Cvetnić, M.; Kučić Grgić, D.; et al. Evaluation of fenton, photo-fenton and fenton-like processes in degradation of PE, PP, and PVC microplastics. *Water* **2024**, *16*, 673. https://doi.org/10.3390/w16050673.
23. Topkaya, E.; Arslan, A.; Veli, S.; Kuru, S.; Sezer, M. Removal of microplastics by ozone oxidation from urban wastewater using taguchi experimental design. *Water Air Soil Pollut.* **2025**, *236*, 606. https://doi.org/10.1007/s11270-025-08249-8.
24. Xiao, Y.; Tian, Y.; Xu, W.; Zhu, J. Photodegradation of microplastics through nanomaterials: Insights into photocatalysts modification and detailed mechanisms. *Materials* **2024**, *17*, 2755. https://doi.org/10.3390/ma17112755.
25. Roy, H.; Mahmud, F.; Sarker, D.; Banhi, T.S.; Sharmin, U.; Roy, B.N.; Islam, M.S. Degradation of Microplastics in Aquatic Environments through an Advanced Oxidation Process. In *Handbook of Microplastic Pollution in the Environment*, 1st ed.; CRC Press: Boca Raton, FL, USA, 2025; p. 31.

26. Kumar, A.; Indhur, R.; Bux, F.; Kumari, S. Recent advances in mechanistic insights into microplastics mitigation strategies via emerging advanced oxidation processes: Legislation, challenges, and future direction. *Sci. Total Environ.* **2024**, *957*, 177150. https://doi.org/10.1016/j.scitotenv.2024.177150.
27. Navarro-García, Á.; Gómez, M.; Murcia, M.D.; Gómez, E.; Hidalgo, A.M.; Dorado, L.A.; Bastida, J. Photodegradation of Polyethylene Terephthalate and Bis(2-hydroxyethyl) Terephthalate Using Excimer Lamps and Hydrogen Peroxide: A Strategy for PET–Derived Waste Treatment. *Molecules* **2025**, *30*, 3302. https://doi.org/10.3390/molecules30153302.
28. Sosnin, E.A.; Oppenländer, T.; Tarasenko, F.V. Applications of capacitive and barrier discharge excilamps in photoscience. *J. Photochem. Photobiol. C* **2006**, *7*, 145–163. https://doi.org/10.1016/j.jphotochemrev.2006.12.002.
29. Matafonova, G.; Christofi, N.; Batoev, V.; Sosnin, E. Degradation of chlorophenols in aqueous media using UV XeBr excilamp in a flow-through reactor. *Chemosphere* **2008**, *70*, 1124–1127. https://doi.org/10.1016/j.chemosphere.2007.08.022.
30. Murcia, M.D.; Gómez, M.; Gómez, E.; Gómez, J.L.; Christofi, N. Photodegradation of congo red using XeBr, KrCl and Cl_2 barrier discharge excilamps: A kinetics study. *Desalination* **2011**, *281*, 364–371. https://doi.org/10.1016/j.desal.2011.08.011.
31. Murcia, M.D.; Gómez, M.; Gómez, E.; Gómez, J.L.; Hidalgo, A.M.; Murcia, S.; Campos, D. Comparison of two excilamps and two reactor configurations in the UV-H_2O_2 removal process of amaranth. *J. Water Process Eng.* **2020**, *33*, 101051. https://doi.org/10.1016/j.jwpe.2019.101051.
32. Tchaikovskaya, O.N.; Karetnikova, E.; Murcia, M.D.; Gómez, M.; Gómez, J.L. Photodegradation of 2-methyl-4-chlorophenol in a KrCl exciplex flow-Through photoreactor: A kinetic study. *Desalin. Water Treat.* **2015**, *54*, 1862–1871. https://doi.org/10.1080/19443994.2014.891079.
33. Gonzalez, D.H.; Kwang, X.M.; Scott, J.A.; Paulson, S.E. Terephthalate Probe for Hydroxyl Radicals: Yield of 2-Hydroxyterephthalic Acid and Transition Metal Interference. *Anal. Letters* **2018**, *51*, 2488–2497. https://doi.org/10.1080/00032719.2018.1431246.
34. Camacho-Gonzalez, M.A.; Hernandez-Reyes, A.; Garrido-Hernandez, A.; Olivares-Xometi, O.; Likhanova, N.V.; Lijanova, I.V. TPA and PET Photo-Degradation by Heterogeneous Catalysis Using a $(Al_2O_3)_{0.75}TiO_2$ Coating. *Water. Sci. Technol.* **2025**, https://doi.org/10.20944/preprints202503.2121.v1.
35. Brame, J.; Long, M.; Li, Q.; Alvarez, P. Inhibitory effect of natural organic matter or other background constituents on photocatalytic advanced oxidation processes: Mechanistic model development and validation. *Wat. Res.* **2015**, *84*, 362–371. https://doi.org/10.1016/j.watres.2015.07.044.